

Finger abduction trajectory prediction from high-density ECoG

Abstract.

Objective A case study is conducted to show that not only finger flexion- but also finger abduction trajectories can be decoded from high-density electrocorticography (ECoG) recordings.

Approach Two patients, temporarily implanted with high-density ECoG grids as part of their clinical workup, performed a cued single finger flexion task, a cued sign language alphabet task and a cued finger abduction task. The extended Block-Term Tensor Regression (eBTTR) model was adopted to predict finger trajectories after being developed on simultaneous data glove/ECoG recordings. The model performance on the single finger flexion task provides a reference for comparing that on the finger abduction task. Finally, the sign language alphabet task involves realistic, complex finger movements, calling upon both finger flexions and abductions.

Main results We show that finger abduction trajectories can be decoded from ECoG recordings, with comparable precision as single finger flexion trajectories, and even when expressing sign language gestures that involve joint finger flexions and abductions.

Significance Our findings show for the first time that finger abduction trajectories can be decoded from ECoG even when part of Sign Language Alphabet gestures.

Submitted to: *J. Neural Eng.*

1. Introduction

Diseases that cause injury to descending motor-neuron tracts in the brain stem, such as amyotrophic lateral sclerosis (ALS) and brainstem stroke, or a cervical injury due to an accident can leave individuals paralysed with little-to-no voluntary muscle control. Motor brain computer interfaces (BCIs) can bypass defective neural pathways to replace the function of a lost or impaired body part. This has led to several pre-clinical milestones including the control of prosthetic hands, arms or other effectors [1, 2, 3, 4, 5, 6, 7]. These studies rely on microelectrode arrays (MEAs) implanted in the cortical tissue as they provide recordings with high temporal and spatial resolution - even down to individual neurons - enabling motor control with several degrees of freedom. However, as the electrodes enter the cortical tissue, putatively causing irreversible damage to its vasculature, the evoked fibrous scar tissue formation affects long-term signal stability, calling for regular decoder recalibrations, and thus dedicated time from the user, on top of brain plasticity processes [8].

Electrocorticography (ECoG) has garnered attention within the motor-BCI community. ECoG involves the placement of electrodes on the exposed cortical surface to record electrical activity. Compared to other implant types, ECoG offers a broader coverage of the cortical surface, enhanced long-term signal stability [9, 10], superior spatial resolution compared to electroencephalography (EEG) [11], and a more extensive spectral bandwidth with increased signal amplitude [12]. Various studies [13, 14, 15, 16, 17, 18, 19] have highlighted the potential of ECoG signals from the primary motor cortex in decoding continuous arm trajectories, as they exhibit distinctive motor-related spatio-temporo-spectral patterns [20, 14, 21]. Stunning recent successes with ECoG implants are the control of individual fingers with a modular prosthetic limb [1], and four-limb- [19] or bi-manual exoskeletons [22] and lower limb muscles by the electrical stimulation of the corresponding spinal cord regions [23]. However, the decoding of more subtle muscular activity such as finger gestures is an outstanding challenge, for example, the decoding of rapid and coordinated finger movements, such as object grasping and hand gestures. This necessitates further algorithmic developments. Progress in finger movement decoding owes to joint ECoG and data

glove recordings in temporarily-implanted, able-bodied individuals, mostly focal epilepsy patients monitored for seizure localisation during their presurgical workup. For example, Kubanek et al. [24] focused on continuous decoding of individual finger flexions and extensions using motor potentials (LMP) and spectral amplitudes across five frequency bands.

Previous research has demonstrated the successful decoding of finger flexion movements from ECoG signals ([19, 25, 26, 27, 28, 29, 30]). Block-Term Tensor Regression (BTTR), as detailed in [31] and [32], was recently introduced for ECoG-based finger flexion decoding. The main algorithmic principle behind BTTR is Tucker decomposition. Block-Term refers to a deflation scheme that generates blocks with varying multilinear Tucker ranks. Originally, BTTR predicted single finger trajectories only, but extended BTTR (eBTTR) lifted this limitation so that coordinated finger movements could be predicted, including finger co-activations i.e. unintentional finger movements [33]. While, in principle, one could stack BTTR models of individual fingers, it will fall short in addressing the temporal overlap and spatial sparsity ECoG signals exhibit during coordinated finger flexions [34].

The aforementioned studies focused on finger flexions, which is useful for applications such as grasping a cup. However, when aiming for restoring hand dexterity, finger abduction becomes important as well. Although the accurate prediction of finger abduction trajectories from (high-density) ECoG could have a significant impact on the development of hand motor BCIs, it received less attention.

Some studies tangentially refer to finger abduction as part of two-dimensional finger movements. In [35] an intracortical BCI was developed to decode attempted handwriting movements from micro-electrode implants in a paralyzed individual's hand knob area. Patients were instructed to imagine they were holding a pen and were writing on (ruled) paper. In [16] middle finger movements were decoded from ECoG to control a cursor in two dimensions, which involve both finger flexion and abduction. However, the said studies do not directly investigate the decoding of finger abduction.

Hu and colleagues ([36]) investigated finger movement recognition via high-density surface electromyography (HD-sEMG). Their study involved 20 healthy subjects

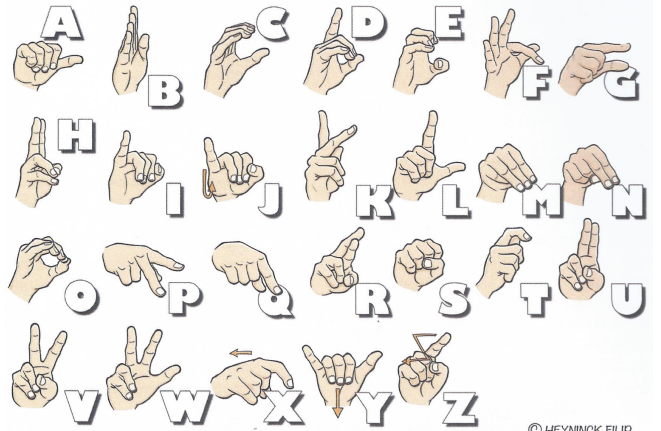
and, using a 22-sensor dataglove, had them perform various finger movements including finger flexion and finger abduction. They found that finger abduction could be decoded similarly to finger flexions.

Finger flexion papers are numerous mostly based on the open access Stanford ECoG library [37] with recordings of repetitive performed single finger flexions and 2 gestures - fist clenching and pinching -, and imagined fist clenching, and the BCI Competition IV data set [38] of repetitive performed single finger flexions (now part of the Stanford library). The authors of those papers always try to better than previous reports, possibly leading to an overanalysis of the same data set. We preferred to collect our own data. This could explain the differences in correlation coefficients. There are much less reports on distinguishing finger flexion from extension [39], sustained flexion and coordinated finger movements such as grasping, other whole hand gestures (e.g scissors, rock, and paper, [40, 34, 41]), finger tapping [1] and sign language gestures [42, 43].

We propose to decode the finger trajectories that underlie the expression of letters of the sign language alphabet rather than to classify them. Sign language gestures are expressive signs requiring various coordinated finger actions, synergistic as well as non-synergistic ones, and even abduction, which has not yet been considered in the ECoG literature.

In order to investigate finger abduction decoding from high-density ECoG, a case study was conducted involving subjects performing three different tasks: a cued single finger flexion task, a cued sign language gesture alphabet task, and a cued finger abduction task. The cued single finger flexion task served as a reference to compare the performance of finger flexion decoding with finger abduction decoding. By analyzing the ECoG data, the study aimed to determine if finger abductions could be decoded with a similar level of accuracy as finger flexions as claimed by [36] albeit using HD s-EMG recordings. Furthermore, the sign language gesture alphabet task provided an opportunity to investigate the decoding of complex finger movements that involve both flexions and abductions. The dataset used in this study consisted of ECoG recordings from two patients who performed all gestures of the Flemish Sign Language Alphabet (see Figure 1), as well as explicit finger abduction movements. The eBTTR algorithm was employed as the decoding model [33]. The findings demonstrate that single finger abductions as well as complex hand gestures from the Sign Language Alphabet can be decoded from ECoG. The results indicate that finger abductions can be decoded with a similar level of precision as single finger flexions.

This suggests that ECoG signals hold promise for predicting finger abduction trajectories, expanding the potential applications of BCIs for controlling hand prosthetics and exoskeletons and for promoting neurorehabilitation.



© HEYNINCK FILIP

Figure 1: Flemish sign language alphabet [44] with the corresponding finger movements.

2. Materials and Methods

2.1. Datasets and Tasks

The dataset originates from two patients undergoing treatment of refractory neuropathic facial pain with epidural electrocorticography (ECoG) grids placed on part of the somatosensory and motor cortex. Ethics approval for this study was granted by the Ethics Committee Research UZ/KU Leuven (EC Research). The first patient had an epidural ECoG grids implanted on the right hand-knob area, while the second patient had an epidural grid placed on the left subcentral gyrus and Broca area, and one on the right hand-knob area (refer to Table 1 and Figures 3, 4 and 5).

Three tasks were performed (subject 2 participated in tasks 2 and 3 only). Task 1 involved single finger movements, in which case subject 1 received a cue to start flexing a specific finger with its trajectory measured using a 5DT 14 Ultra data glove (5DT Inc., Irvine, USA), see Figure 2. On average, subject 1 was instructed to flex the prompted finger once for 1 to 2 seconds, followed by a rest period lasting 2 seconds. A total of 150 trials were conducted in a single session lasting 600 seconds, with 30 trials for each finger. In Task 2, both subjects were cued to replicate each of the 26 letters of the Flemish sign language alphabet, cued in randomized order using a hand avatar, with the finger trajectories being measured using the said data glove. Given the location of the experiment

Table 1: Patient Information Leuven dataset

	Subject 1	Subject 2
Age	58	41
Gender	Female	Female
Handedness	Right	Right
Region of pain	Trigeminus neuralgia (left)	Temporomandibular joint disorder, bilateral pain mostly in jaws.
Number of grids	1	2
Type of grid	Medtronic Inc Specify® SureScan® MRI 5-6-5 grid (in-line spacing 4.5 mm, row spacing 1.0 mm, electrode size 1.5 mm x 4.0 mm)	2X Medtronic Inc Specify® SureScan® MRI 5-6-5 grid, in-line spacing 4.5 mm, row spacing 1.0 mm, electrode size 1.5 mm x 4.0 mm
Implanted hemisphere	Right	Left and right
ECoG Grid location	Medial frontoparietal, covering M1 and S1, face and lip area	Left: Lateral frontoparietal, inferior parietal cortex and Broca (Brodmann area 44, inferior frontal gyrus pars opercularis left), Right: Medial frontoparietal, covering M1, S1 hand knob & PMDc
Total number of included electrodes	16	32
Number of electrodes over M1	3	Left: 2, Right: 3
Number of electrodes over S1	4	Left: 5, Right: 4

in Flanders (Belgium), the Flemish Sign Language alphabet was utilized. In Task 3, the two subjects were cued again using a hand avatar, to perform a specific finger abduction pattern, i.e., spreading of two adjoining fingers as wide as possible, again with the finger trajectories being recorded using the same data glove. A total of 120 trials were conducted in a single session lasting 480 seconds, with 30 trials for each abduction. On average, subjects were directed to perform the specified abduction (using an avatar) once for 1 to 2 seconds, followed by a rest period lasting 2 seconds.

2.2. (extended) Block-Term Tensor Regression

(extended) Block-Term Tensor Regression (BTTR) decomposes the input tensor into block components, facilitating efficient regression on high-dimensional data. It effectively captures the underlying structure of the data, making it suitable for applications involving multi-modal datasets [32, 33]. An overview of the mathematical notation used can be found in Table 2.

The proposed regression model is based on Block Term Decomposition (BTD) with automatic MTR determination, denoted as (L_1^k, \dots, L_N^k) . This model employs a deflation-based approach to sequentially Tucker-de-

compose an ECoG tensor and a Finger Movement matrix into a sequence of blocks. By using Automatic Component Extraction (ACE), each block comprises representations maximally correlated.

Given a set of training data $\underline{\mathbf{X}}_{\text{train}} \in \mathbb{R}^{I_1 \times \dots \times I_N}$ and a vectorial response $\mathbf{Y}_{\text{train}} \in \mathbb{R}^{I_1 \times M}$, training aims to automatically identify \mathbf{K} blocks.

$$\underline{\mathbf{X}}_{\text{train}} = \sum_{k=1}^K \underline{\mathbf{G}}_k \times_1 \mathbf{t}_k \times_2 \mathbf{P}_k^{(2)} \times_3 \dots \times_N \mathbf{P}_k^{(n)} + \underline{\mathbf{E}}_k$$

$$\mathbf{Y}_{\text{train}} = \sum_{k=1}^K \mathbf{u}_k \mathbf{q}_k^T + \mathbf{F}_k \text{ with } \mathbf{u}_k = \mathbf{t}_k b_k$$

Here, $\underline{\mathbf{G}}_k \in \mathbb{R}^{1 \times R_2^k \times \dots \times R_N^k}$ represents the core tensor of the k-th block, $\mathbf{P}_k^{(n)}$ represents the loading matrix for the n-mode of the k-th block, \mathbf{u}_k and \mathbf{t}_k are the latent components, \mathbf{q}_k is the loading matrix, b_k is the regression coefficient, and $\underline{\mathbf{E}}_k$ and \mathbf{F}_k represent residuals. Once the model is trained, and the values of $\underline{\mathbf{G}}_k$, $\mathbf{P}_k^{(n)}$, and b_k are computed, the final prediction is obtained as follows: $\mathbf{Y}_{\text{test}} = \mathbf{TZ} = \underline{\mathbf{X}}_{\text{test}(1)} \mathbf{WZ}$, where each column $\mathbf{w}_k = (\mathbf{P}_k^{(n)} \otimes \dots \otimes \mathbf{P}_k^{(2)}) \text{vec}(\underline{\mathbf{G}}_k)$ and each row $z_k = b_k \mathbf{q}_k$.

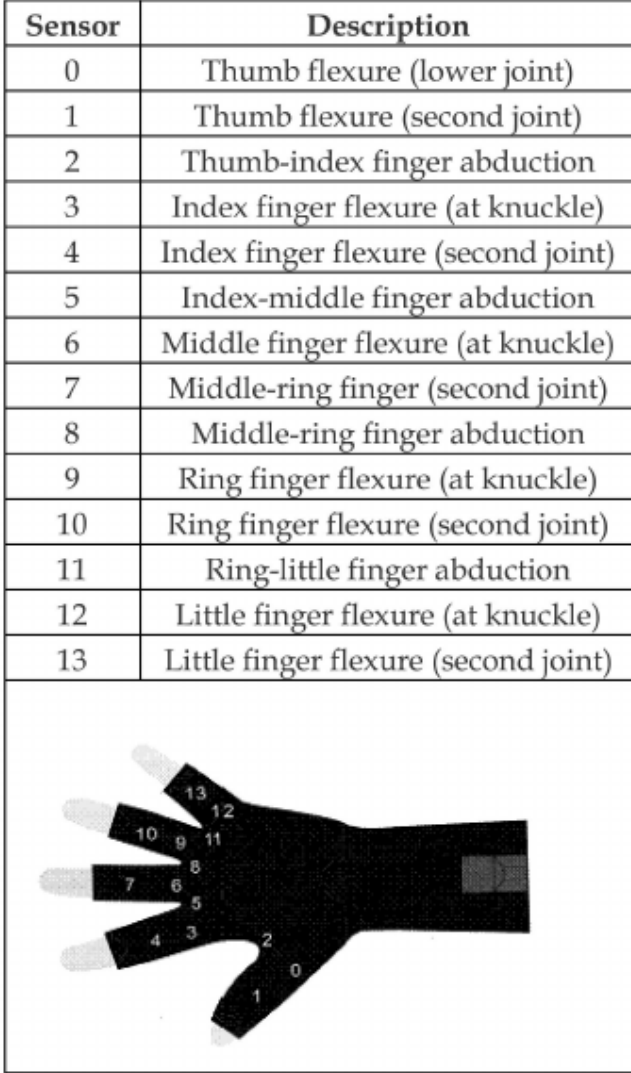


Figure 2: Visual representation of the data glove used in the experiments with the placement of the sensors on the fingers indicated. The flexion sensor closest to the knuckle was used for finger flexion. The abduction sensors were used to record finger abduction.

2.3. Processing

Notch filters, centered at 50 and 100 Hz, were employed to eliminate power line noise. Subsequently, a visual inspection of the data was conducted to identify and eliminate faulty channels. A channel was flagged as problematic if it displayed an unstable or unchanging signal. Following this, Common Average Reference (CAR) re-referencing was applied by subtracting the average signal from all signals [45]. Finally, the electrocorticography (ECoG) signals were structured into a 4th-order ECoG tensor $\mathbf{X} \in \mathbb{R}^{\text{Samples} \times \text{Channels} \times \text{Frequencies} \times \text{Time}}$. In this representation, **Samples** corresponds to the time

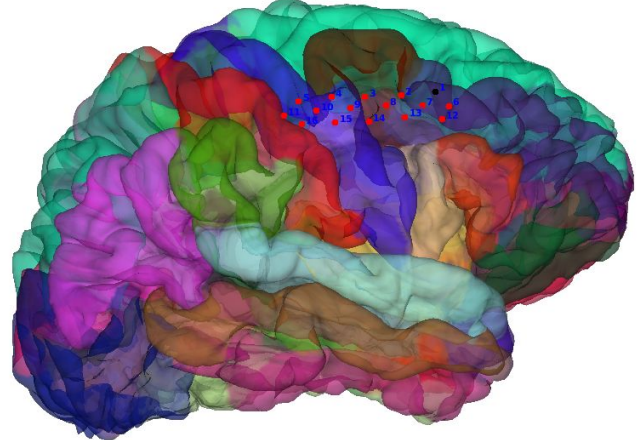


Figure 3: Visual representation of the ECoG grid placement on the right hand-knob area of subject 1.

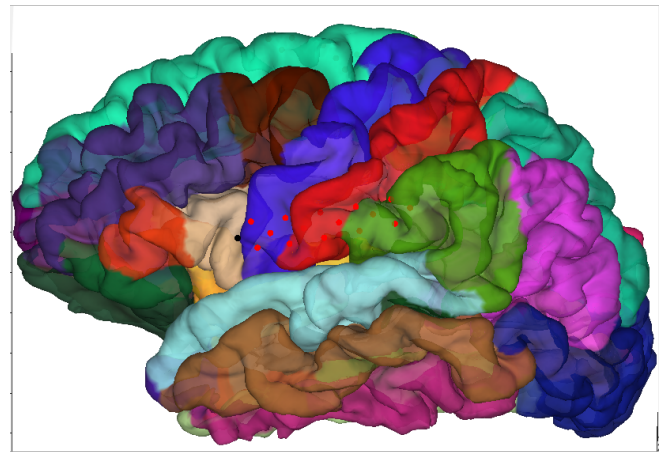


Figure 4: Visual representation of the ECoG grid placement on the left subcentral gyrus and Broca area of subject 2.

instants to be decoded (i.e. the time that data was sampled from the glove, corresponding to entries in the matrix $\mathbf{Y} \in \mathbb{R}^{\text{Samples} \times \text{Fingers}}$, and **Channels** reflects the number of electrodes remaining after the removal of faulty channels. **Frequencies** encompasses 16 components, including 15 gamma band powers and the local motor potential (**LMP** [46, 31]). The gamma band powers were extracted in the 60 to 130 Hz range (high-frequency bands) using 10 Hz frequency bands with 5 Hz overlap, using bidirectional third-order Butterworth band-pass filters [47]. The LMP was determined by extracting amplitudes in the 0.1 to 1.5 Hz range. **Time** comprises 10 instances derived from the most recent 1-second epoch, achieved by downsampling each of the 16 band-pass filtered ECoG signals to 10 Hz. The preprocessing steps are as

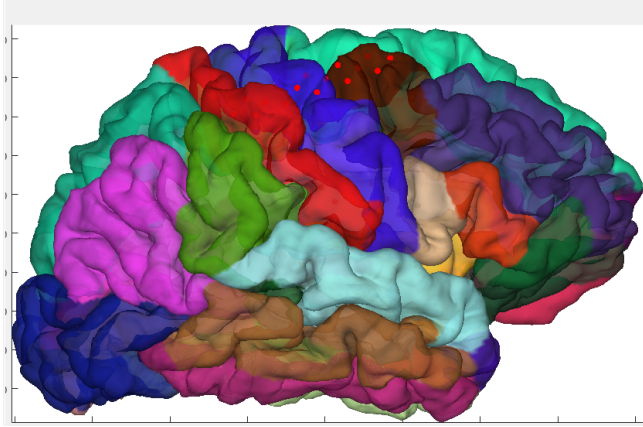


Figure 5: Visual representation of the ECoG grid placement on the right hand-knob area of subject 2.

Table 2: Mathematical notation

Notation	Description
$\underline{\mathbf{T}}, \mathbf{M}, \mathbf{v}, S$	tensor, matrix, vector, scalar (respectively)
\mathbf{M}^T	transpose of matrix
\times_n	mode-n product between tensor and matrix
\otimes	Kronecker product
\circ	outer product
$\ \cdot\ _F$	Frobenius norm
$\mathbf{T}_{(n)}$	mode-n unfolding of tensor $\underline{\mathbf{T}}$
$\underline{\mathbf{C}}^{(T)}$	core tensor associated to tensor $\underline{\mathbf{T}}$
$\mathbf{M}^{(n)}$	mode-n factor matrix
\mathbf{M}_{ind}	(sub-)matrix including the column(s) indicated in ind
$\mathbf{M}_{\setminus ind}$	(sub-)matrix excluding the column(s) indicated in ind
$[\underline{\mathbf{C}}; \mathbf{M}^{(1)}, \dots, \mathbf{M}^{(N)}]$	full multilinear product $\underline{\mathbf{C}} \times \mathbf{M}^{(1)} \times_2 \dots \times_N \mathbf{M}^{(N)}$
$\langle \underline{\mathbf{T}}, \underline{\mathbf{E}} \rangle_{\{n,n\}}$	mode-n cross-covariance tensor

follows:

- Normalize (i.e., z-score) data glove data independently for each finger $\mathbf{Y} \in \mathbb{R}^{\text{Samples} \times \text{Fingers}}$.
- Apply epoch selection for each channel using the past second for band-pass filtering, followed by a downsampling to 10 Hz. This process yields the frequency and time dimensions for each sample and channel.
- Normalize (i.e., z-score) the tensor according to

the channel and frequency bands of the training set, with the same parameters applied to the test set.

- Merge the channel matrices into $\underline{\mathbf{X}} \in \mathbb{R}^{\text{Samples} \times \text{Channels} \times \text{Frequencies} \times \text{Time}}$

The resulting preprocessed data is then utilized in extended Block Term Tensor Regression (eBTTR), a regression model specifically designed to accommodate the multilinear nature of human intracranial finger movement recordings. The model relies on recursive Tucker decomposition combined with automatic component extraction [32, 33]. A 5-fold cross-validation approach was used to determine the optimal number of Tucker blocks and a separate test set to determine model performance. For each of the three tasks, a separate eBTTR model is trained. This also allows for cross-testing, i.e. use an eBTTR model trained on task 1 (single finger) to decode task 2 (joint finger).

Model performance is expressed in terms of the Pearson correlation coefficient between the glove-recorded finger trajectories and the predicted ones. The test dataset was partitioned into five non-overlapping blocks. For assessing the significance of differences in average accuracies across various fingers and subjects, we employed the Wilcoxon signed-rank test (two-tailed) [48]; a results with a p-value smaller than 0.05 was considered significant.

2.4. Non-multilinear approaches

Additionally, we will compare the performance of eBTTR with that of other contemporary approaches, Random Forests (RF), Convolutional Neural Networks (CNN), and Long Short-Term Memory Networks (LSTM), as proposed and evaluated in [30]. Notably, these models are non-multilinear ones.

However, it is important to note that in both [28] and [30], only a single test set was used to evaluate model performance. This methodological limitation restricts the possibility of performing statistically rigorous significance testing between the competing algorithms. To overcome this limitation and ensure robust comparisons, we have re-implemented the AM, RF, LARS, CNN, and LSTM models. Our approach ensures a fair and reliable performance evaluation across multiple test sets. The detailed steps for each implementation are described below.

For the AM-based method, we followed the procedure outlined in [28]. First, the ECoG signals were filtered into three distinct frequency bands: sub-gamma (1-60Hz), gamma (60-100Hz), and high-gamma (100-200Hz). For each of these bands, we computed the amplitude modulation (AM) and derived their respective band-specific AM features. These features were then

subject to a feature selection process, where forward feature selection using a wrapper approach was applied to identify the most relevant AM features for each individual subject and finger. The selected features were subsequently used to fit a linear regression model. Finally, we assessed the performance of the model and compared it against the results originally reported in [28] to ensure consistency.

For the LARS model, we employed the *LassoLars* function from the most recent version of the *scikit-learn* Python package (version 0.24.2, released in April 2021). Although Xie et al. did not explicitly state the version they used, we assume they used version 0.19.1, as that would have been current during their research. In our implementation, LARS first transforms the original signal using Independent Component Analysis (ICA), decomposing the signal into different frequency bands. From these bands, the band powers were computed, and a LassoLars regression model was subsequently fitted. The primary tuning parameter for LARS is α , which determines the weight of the penalty term, where $\alpha = 0$ corresponds to ordinary least squares (OLS) regression. We employed a line search technique to optimize the α parameter for best performance.

Similarly, for the Random Forest (RF) model, we adopted an analogous preprocessing pipeline. We used the *RandomForestRegressor* function from the same version of the *scikit-learn* package. Like LARS, RF also performs signal decomposition using ICA and band power calculation. The processed features were then used to train the *RandomForestRegressor* model.

For the CNN and LSTM models, we followed the architectural specifications and training procedures provided in [30]. The CNN model applies a linear regression model to the features extracted using a convolutional neural network, whereas the LSTM model uses a recurrent network to capture temporal dependencies in the data. Both models were implemented using the PyTorch framework in Python (version 1.8.0, released in March 2021), although Xie et al. did not specify the version of PyTorch used in their experiments.

By re-implementing these methods and testing them on multiple datasets, we aim to provide a more robust comparison, overcoming the limitations of previous single-test-set studies.

3. Results

3.1. Per-task analysis

Figure 6 illustrates the relationship between the raw recordings, the ground truth (data glove), the features extracted from the ECoG data (frequency fea-

tures, LMP, time features) and the predicted trajectory. Table 3 summarizes the finger flexion results of Task 1 and 2. Note that Task 1 was performed by subject 1 only. Task 2 considers all gestures of the sign language alphabet, thus going beyond the selection of 4 gestures of the Utrecht experiment [42].

For Task 1, Subject 1 shows higher correlation coefficients for the thumb, index and ring fingers compared to the other fingers. For task 2, both subjects exhibit varying correlation coefficients across different fingers, with mostly higher coefficients for Subject 2.

Table 4 summarizes the finger abduction results of Task 3. The results reveal distinctive correlation patterns for specific finger pairs, with Subject 2 exhibiting overall stronger correlations, especially for the Middle-Ring and Ring-Pinky pairs. Comparing the Task 2 (finger gestures), the same fingers flexed individually also yield stronger correlations. It seems, thus, that finger flexions and finger abductions yield similar decoding accuracies. The exception is the Thumb as it features the lowest abduction decoding accuracy for both subjects but a good flexion decoding performance during finger gesture movements. We expect that this due to the difficulty to accurately gauge Thumb abductions vs. flexions with the data glove (the abduction of the listed fingers pairs is measured by dedicated sensors unlike the thumb).

The abduction results also show that the decoding with eBTTR of finger abductions gives better results compared to other contemporary methods (Table 4). The Wilcoxon signed-rank test was used to compare the performance of eBTTR with the other methods. The results show that eBTTR significantly outperforms the other methods for all finger pairs ($p < 0.05$).

Chance level was computed for the eBTTR model for each finger pair by randomly shuffling the LMP, and other frequency bands and by taking the 90th percentile of the correlation coefficients. The results show that the eBTTR model significantly outperforms the chance level for all finger pairs ($p < 0.05$).

The decoders applied to the dataset exhibit significantly lower correlation coefficients than initially expected. This is because the dataset was recorded with epidural electrodes whereas typical datasets are recorded with subdural electrodes. Epidural recordings exhibit lower signal amplitudes than their subdural counterpart, particularly when using high-density grids, and this can lead to lower finger trajectory correlations ([49]).

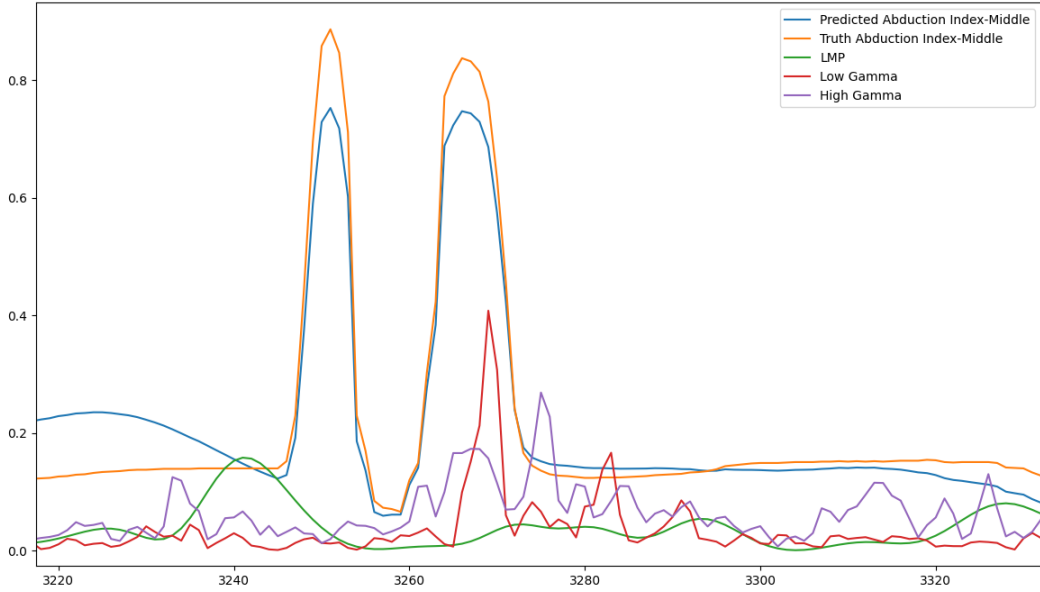


Figure 6: Raw recording of a single electrode for the activity of the thumb-index finger of subject 2 (Task 2) along with LMP, low and high gamma amplitude and the predicted trajectory. Y-axis is in arbitrary units, X-axis in ms. Color of the curves as indicated in the insert.

Methods	Thumb	Index	Middle	Ring	Pinky
Single Finger Subject 1	0.31 ± .05	0.45 ± .07	0.12 ± .04	0.23 ± .02	0.16 ± .01
Finger Gesture Subject 1	0.42 ± .05	0.32 ± .07	0.38 ± .04	0.23 ± .02	0.12 ± .01
Finger Gesture Subject 2	0.32 ± .05	0.46 ± .07	0.49 ± .04	0.32 ± .02	0.33 ± .01

Table 3: Pearson correlation coefficients of cued single finger movement and finger gesture trajectories.

Methods	Thumb-Index	Index-Middle	Middle-Ring	Ring-Pinky
eBTTR S1	0.14 ± .05	0.32 ± .07	0.28 ± .04	0.22 ± .01
eBBTR Chance S1	-0.02 ± .02	0.01 ± .03	0.01 ± .02	-0.01 ± .01
AM S1	0.03 ± .03	0.11 ± .03	0.14 ± .03	0.14 ± .04
RF S1	0.02 ± .04	0.07 ± .02	0.08 ± .05	0.06 ± .04
LARS S1	0.08 ± .03	0.10 ± .03	0.09 ± .03	0.08 ± .03
CNN S1	0.11 ± .01	0.24 ± .03	0.21 ± .01	0.22 ± .03
LSTM S1	0.12 ± .02	0.32 ± .03	0.22 ± .02	0.20 ± .02
eBTTR S2	0.04 ± .05	0.36 ± .08	0.37 ± .04	0.37 ± .01
AM S2	0.02 ± .03	0.09 ± .03	0.11 ± .03	0.11 ± .04
RF S2	0.01 ± .04	0.06 ± .02	0.07 ± .05	0.05 ± .04
LARS S2	0.07 ± .03	0.09 ± .03	0.08 ± .03	0.07 ± .03
CNN S2	0.10 ± .01	0.23 ± .03	0.20 ± .01	0.21 ± .03
LSTM S2	0.11 ± .02	0.31 ± .03	0.21 ± .02	0.19 ± .02

Table 4: Pearson correlation coefficients of cued finger abduction movement compared between eBTTR and several non-multilinear algorithms (see text for their description). Significantly different results compared eBTTR are indicated in bold. S1 = subject 1, S2 = subject 2

3.2. Cross-task analysis

Since subject 1 performed both Task 1 and 2, a cross-task analysis was performed. Hereby, an eBTTR model

Methods	Thumb	Index	Middle	Ring	Pinky
Trained T.1 / Test T.2	0.22 ± .06	0.12 ± .02	0.21 ± .05	0.08 ± .02	0.09 ± .02
Trained T.2 / Test T.1	0.28 ± .03	0.27 ± .04	0.07 ± .01	0.21 ± .02	0.15 ± .01

Table 5: Pearson correlation coefficients of cued single finger movement and finger gesture trajectories (for Subject 1).

was trained on the data of Task 1 and tested on Task 2 and vice-versa. The results are summarized in Table 5. The performance of the model trained on single finger movements is significantly lower compared to the performance of the model trained on joint finger movements (see Table 3).

4. Discussion

We reported on two patients implanted with epidural ECoG over the somatomotor cortex when performing the following tasks: 1) cued single finger flexion (patient 1 only), 2) visually cued sign language gestures, and 3) visually cued finger abductions. For each task separately eBTTR models were trained to decode the data glove-recorded finger trajectories, and model performance was measured as the Pearson correlation coefficient between predicted- and data glove-recorded finger trajectories.

Decoding coordinated finger flexion movements from ECoG has only been sparsely addressed and mostly restricted to regressing [50, 51] or classifying 1 or 2 types of grasping [52, 53, 54, 55] and classifying 3 to 4 whole hand gestures [34, 40, 41, 42, 43]. To the best of our knowledge, there exists no prior reports on decoding, abduction or adduction of all fingers of the (dominant) hand from ECoG with the exception of thumb abduction/adduction from microelectrode array recordings [39]. Our novelty is to show that decoding finger abductions can be predicted from ECoG with comparable accuracy to finger flexion except for the thumb which could be due to the data glove sensors (abduction of adjoining fingers pairs is measured by dedicated sensors unlike the thumb, Figure 2).

We also showed the accuracy of a decoder trained on single-finger flexion when applied to coordinated-finger flexion (Table 5). This was motivated by evidence that single-finger movements and coordinated ones share a common cortical network [56]. However, the performance was in our case significantly lower, which connects to our earlier finding using the eBTTR decoder trained on the BCI Competition IV (dataset 4) comprising subdural ECoG recordings from 3 subjects [33], and to the findings of Kuo et al. [51] using a CNN decoder trained on propriety subdural micro-ECoG recordings from 2 subjects. The inverse case of a decoder trained on coordinated-finger flexion but tested on single-finger flexion seemed to perform on par, calling for all finger decoders such as eBTTR.

Our linear decoder eBTTR performed better or was on par with non-linear decoders, including deep learning ones, when trained and tested on the same data set (Table 4). ECoG recordings are predominantly recorded during the clinical workup of a surgical intervention and therefore limited in size, which in turn is expected to limit the performance of the more data devouring deep learning approaches. In order to remedy the data size issue, recently several approaches have been developed that allow decoder training on pooled multi-subject data (transfer learning). As ECoG grid placement is clinically motivated and highly variable between patients, these approaches rely on spatial coding schemes (spatial embeddings) to address the cross-subject electrode alignment issue present in ECoG as well as stereotactic EEG settings [57, 58], possibly followed by a fine-tuning session on the targeted subject to further improve accuracy. In principle, the electrode-dimension of eBTTR’s input tensor could be remapped to brain regions of interest thereby accounting for the electrode distance to these regions as in [57]. Another possibility is to pretrain a transformer on pooled multi-subject data [59], to learn the non-linear trans-

formation of the intracranial recordings, followed by eBTTR, with the latter fine-tuned to the targeted subject. However, in that case eBTTR loses the benefit of the multilinear structure of ECoG data. It is also unclear whether transfer learning schemes would be precise enough to account for the more fine-grained finger trajectory predictions, thus going beyond the classification of e.g. limb movements. This is a topic for future research.

Although the abduction results are encouraging, we acknowledge a number of limitations of our study. We showed results from 2 patients undergoing treatment of refractory neuropathic facial pain with somatomotor implants. The largest group are the focal epilepsy patients but they have their implants primarily on the temporal lobe given that temporal lobe epilepsy the most common form of focal epilepsy (<https://www.epilepsy.com/what-is-epilepsy/syndromes/temporal-lobe-epilepsy>). Furthermore, as our patients were implanted with epidural electrodes, and despite such recordings do not seem to affect movement classification accuracy [49, 60], the lower signal amplitudes affected our finger trajectory correlations. Finally, although small differences in correlations between our 2 patients were observed, possibly attributable to differences in electrode locations, our study could benefit from additional ECoG recordings preferably from hand motor-area implanted subdural electrode grids.

5. Conclusion

We presented a comprehensive investigation into the prediction of finger abduction trajectories from high-density ECoG data. The study demonstrates the feasibility of decoding finger abductions using the eBTTR algorithm and shows a decoding performance that is comparable to finger flexion except for the thumb, possibly due to technical aspects of the used data glove. These findings could contribute to the development of hand prosthetics and exoskeletons and to hand neurorehabilitation.

- [1] Guy Hotson, David P McMullen, Matthew S Fifer, Matthew S Johannes, Kapil D Katyal, Matthew P Para, Robert Armiger, William S Anderson, Nitish V Thakor, Brock A Wester, et al. Individual finger control of a modular prosthetic limb using high-density electrocorticography in a human subject. *Journal of neural engineering*, 13(2):026017, 2016.
- [2] Jennifer L Collinger, Brian Wodlinger, John E Downey, Wei Wang, Elizabeth C Tyler-Kabara, Douglas J Weber, Angus JC McMorland, Meel Velliste, Michael L Boninger, and Andrew B Schwartz. High-performance neuroprosthetic control by an individual with tetraplegia. *The Lancet*, 381(9866):557–564, 2013.
- [3] Dawn M Taylor, Stephen I Helms Tillery, and Andrew B Schwartz. Direct cortical control of 3d neuroprosthetic devices. *Science*, 296(5574):1829–1832, 2002.

- [4] Leigh R Hochberg, Mijail D Serruya, Gerhard M Friehs, Jon A Mukand, Maryam Saleh, Abraham H Caplan, Almut Branner, David Chen, Richard D Penn, and John P Donoghue. Neuronal ensemble control of prosthetic devices by a human with tetraplegia. *Nature*, 442(7099):164–171, 2006.
- [5] Leigh R Hochberg, Daniel Bacher, Beata Jarosiewicz, Nicolas Y Masse, John D Simmeral, Joern Vogel, Sami Haddadin, Jie Liu, Sydney S Cash, Patrick Van Der Smagt, et al. Reach and grasp by people with tetraplegia using a neurally controlled robotic arm. *Nature*, 485(7398):372–375, 2012.
- [6] Marco Vilela and Leigh R Hochberg. Applications of brain-computer interfaces to the control of robotic and prosthetic arms. *Handbook of clinical neurology*, 168:87–99, 2020.
- [7] B Wodlinger, JE Downey, EC Tyler-Kabara, AB Schwartz, ML Boninger, and JL Collinger. Ten-dimensional anthropomorphic arm control in a human brain-machine interface: difficulties, solutions, and limitations. *Journal of neural engineering*, 12(1):016011, 2014.
- [8] Gerwin Schalk. Can electrocorticography (ecog) support robust and powerful brain-computer interfaces? *Frontiers in neuroengineering*, page 9, 2010.
- [9] Wei Wang, Jennifer L Collinger, Alan D Degenhart, Elizabeth C Tyler-Kabara, Andrew B Schwartz, Daniel W Moran, Douglas J Weber, Brian Wodlinger, Ramana K Vinjamuri, Robin C Ashmore, et al. An electrocorticographic brain interface in an individual with tetraplegia. *PloS one*, 8(2):e55344, 2013.
- [10] Ewan S Nurse, Sam E John, Dean R Freestone, Thomas J Oxley, Hoameng Ung, Samuel F Berkovic, Terence J O'Brien, Mark J Cook, and David B Grayden. Consistency of long-term subdural electrocorticography in humans. *IEEE Transactions on Biomedical Engineering*, 65(2):344–352, 2017.
- [11] Kai J Miller, Larry B Sorensen, Jeffrey G Ojemann, and Marcel Den Nijs. Power-law scaling in the brain surface electric potential. *PLoS Comput Biol*, 5(12):e1000609, 2009.
- [12] Richard J Staba, Charles L Wilson, Anatol Bragin, Itzhak Fried, and Jerome Engel Jr. Quantitative analysis of high-frequency oscillations (80–500 Hz) recorded in human epileptic hippocampus and entorhinal cortex. *Journal of neurophysiology*, 88(4):1743–1752, 2002.
- [13] Zenas C Chao, Yasuo Nagasaka, and Naotaka Fujii. Long-term asynchronous decoding of arm motion using electrocorticographic signals in monkey. *Frontiers in neuroengineering*, 3:3, 2010.
- [14] Tonio Ball, Markus Kern, Isabella Mutschler, Ad Aertsen, and Andreas Schulze-Bonhage. Signal quality of simultaneously recorded invasive and non-invasive eeg. *Neuroimage*, 46(3):708–716, 2009.
- [15] Jeroen CW Siero, Dora Hermes, Hans Hoogduin, Peter R Luijten, Nick F Ramsey, and Natalia Petridou. Bold matches neuronal activity at the mm scale: A combined 7 t fmri and ecog study in human sensorimotor cortex. *Neuroimage*, 101:177–184, 2014.
- [16] Gerwin Schalk, Kai J Miller, Nicholas R Anderson, J Adam Wilson, Matthew D Smyth, Jeffrey G Ojemann, Daniel W Moran, Jonathan R Wolpaw, and Eric C Leuthardt. Two-dimensional movement control using electrocorticographic signals in humans. *Journal of neural engineering*, 5(1):75, 2008.
- [17] Takufumi Yanagisawa, Masayuki Hirata, Youichi Saitoh, Haruhiko Kishima, Kojiro Matsushita, Tetsu Goto, Ryohei Fukuma, Hiroshi Yokoi, Yukiyasu Kamitani, and Toshiaki Yoshimine. Electrocorticographic control of a prosthetic arm in paralyzed patients. *Annals of neurology*, 71(3):353–361, 2012.
- [18] Elizabeth A Felton, J Adam Wilson, Justin C Williams, and P Charles Garell. Electrocorticographically controlled brain-computer interfaces using motor and sensory imagery in patients with temporary subdural electrode implants: report of four cases. *Journal of neurosurgery*, 106(3):495–500, 2007.
- [19] Alim Louis Benabid, Thomas Costecalde, Andrey Eliseyev, Guillaume Charvet, Alexandre Verney, Serpil Karakas, Michael Foerster, Aurélien Lambert, Boris Morinière, Neil Abroug, et al. An exoskeleton controlled by an epidural wireless brain-machine interface in a tetraplegic patient: a proof-of-concept demonstration. *The Lancet Neurology*, 18(12):1112–1122, 2019.
- [20] Nicholas R Anderson, Tim Blakely, Gerwin Schalk, Eric C Leuthardt, and Daniel W Moran. Electrocorticographic (ecog) correlates of human arm movements. *Experimental brain research*, 223(1):1–10, 2012.
- [21] David T Bundy, Mrinal Pahwa, Nicholas Szrama, and Eric C Leuthardt. Decoding three-dimensional reaching movements using electrocorticographic signals in humans. *Journal of neural engineering*, 13(2):026021, 2016.
- [22] Alexandre Moly, Thomas Costecalde, Félix Martel, Matthieu Martin, Christelle Larzabal, Serpil Karakas, Alexandre Verney, Guillaume Charvet, Stephan Chabardes, Alim Louis Benabid, et al. An adaptive closed-loop ecog decoder for long-term and stable bimanual control of an exoskeleton by a tetraplegic. *Journal of Neural Engineering*, 19(2):026021, 2022.
- [23] Henri Lorach, Andrea Galvez, Valeria Spagnolo, Felix Martel, Serpil Karakas, Nadine Interling, Molwynn Vat, Olivier Fairvre, Cathal Harte, Salif Komi, et al. Walking naturally after spinal cord injury using a brain-spine interface. *Nature*, pages 1–8, 2023.
- [24] JOJWGSJ Kubanek, Kai J Miller, Jeffrey G Ojemann, Jonathan R Wolpaw, and Gerwin Schalk. Decoding flexion of individual fingers using electrocorticographic signals in humans. *Journal of neural engineering*, 6(6):066001, 2009.
- [25] Qibin Zhao, Cesar F Caiafa, Danilo P Mandic, Zenas C Chao, Yasuo Nagasaka, Naotaka Fujii, Liqiang Zhang, and Andrzej Cichocki. Higher order partial least squares (hpls): a generalized multilinear regression method. *IEEE transactions on pattern analysis and machine intelligence*, 35(7):1660–1673, 2012.
- [26] Andrey Eliseyev and Tetiana Akzenova. Penalized multi-way partial least squares for smooth trajectory decoding from electrocorticographic (ecog) recording. *PloS one*, 11(5):e0154878, 2016.
- [27] Rémi Flamary and Alain Rakotomamonjy. Decoding finger movements from ecog signals using switching linear models. *Frontiers in neuroscience*, 6:29, 2012.
- [28] Nanying Liang and Laurent Bougrain. Decoding finger flexion from band-specific ecog signals in humans. *Frontiers in neuroscience*, 6:91, 2012.
- [29] Zuoguan Wang, Qiang Ji, Kai J Miller, and Gerwin Schalk. Decoding finger flexion from electrocorticographic signals using a sparse gaussian process. In *2010 20th International conference on pattern recognition*, pages 3756–3759. IEEE, 2010.
- [30] Ziqian Xie, Odilia Schwartz, and Abhishek Prasad. Decoding of finger trajectory from ecog using deep learning. *Journal of neural engineering*, 15(3):036009, 2018.
- [31] Flavio Camarrone, Mariana P Branco, Nick F Ramsey, and Marc M Van Hulle. Accurate offline asynchronous detection of individual finger movement from intracranial brain signals using a novel multiway approach. *IEEE Transactions on Biomedical Engineering*, 68(7):2176–2187, 2020.

- [32] Axel Faes, Flavio Camarrone, and Marc M Van Hulle. Single finger trajectory prediction from intracranial brain activity using block-term tensor regression with fast and automatic component extraction. *IEEE Transactions on Neural Networks and Learning Systems*, submitted 2022.
- [33] A Faes and MM Van Hulle. Finger movement and coactivation predicted from intracranial brain activity using extended block-term tensor regression. *Journal of Neural Engineering*, 19(6):066011, 2022.
- [34] Gang Pan, Jia-Jun Li, Yu Qi, Hang Yu, Jun-Ming Zhu, Xiao-Xiang Zheng, Yue-Ming Wang, and Shao-Min Zhang. Rapid decoding of hand gestures in electrocorticography using recurrent neural networks. *Frontiers in neuroscience*, 12:555, 2018.
- [35] Francis R Willett, Donald T Avansino, Leigh R Hochberg, Jaimie M Henderson, and Krishna V Shenoy. High-performance brain-to-text communication via handwriting. *Nature*, 593(7858):249–254, 2021.
- [36] Xuhui Hu, Aiguo Song, Jianzhi Wang, Hong Zeng, and Wentao Wei. Finger movement recognition via high-density electromyography of intrinsic and extrinsic hand muscles. *Scientific Data*, 9(1):373, 2022.
- [37] Kai J Miller. A library of human electrocorticographic data and analyses. *Nature human behaviour*, 3(11):1225–1235, 2019.
- [38] Kai J Miller and Gerwin Schalk. Prediction of finger flexion: 4th brain-computer interface data competition. *BCI Competition IV*, 1:1–2, 2008.
- [39] Matthew S Willsey, Nishal P Shah, Donald T Avansino, Nick V Hahn, Ryan M Jamiolkowski, Foram B Kamdar, Leigh R Hochberg, Francis R Willett, and Jaimie M Henderson. A real-time, high-performance brain-computer interface for finger decoding and quadcopter control. *bioRxiv*, pages 2024–02, 2024.
- [40] Cynthia A Chestek, Vikash Gilja, Christine H Blabe, Brett L Foster, Krishna V Shenoy, Josef Parvizi, and Jaimie M Henderson. Hand posture classification using electrocorticography signals in the gamma band over human sensorimotor brain areas. *Journal of neural engineering*, 10(2):026002, 2013.
- [41] Yue Li, Shaomin Zhang, Yile Jin, Bangyu Cai, Marco Controzzi, Junming Zhu, Jianmin Zhang, and Xiaoxiang Zheng. Gesture decoding using ecog signals from human sensorimotor cortex: a pilot study. *Behavioural neurology*, 2017, 2017.
- [42] Martin G Bleichner, Zachary V Freudenburg, Johannus Martijn Jansma, Erik J Aarnoutse, Mariska J Vansteensel, and Nick Franciscus Ramsey. Give me a sign: decoding four complex hand gestures based on high-density ecog. *Brain Structure and Function*, 221:203–216, 2016.
- [43] Mariana P Branco, Zachary V Freudenburg, Erik J Aarnoutse, Martin G Bleichner, Mariska J Vansteensel, and Nick F Ramsey. Decoding hand gestures from primary somatosensory cortex using high-density ecog. *NeuroImage*, 147:130–142, 2017.
- [44] Filip Heyninck vlaams alphabet gebarentaal. <https://www.filipheyninck.com/illustraties>. Accessed: 2023-04-24.
- [45] Collin D Binnie. *Clinical neurophysiology: EEG, paediatric neurophysiology, special techniques and applications*, volume 2. Elsevier Health Sciences, 2003.
- [46] Aysegul Gunduz, Peter Brunner, Mohit Sharma, Eric C Leuthardt, Anthony L Ritaccio, Bijan Pesaran, and Gerwin Schalk. Differential roles of high gamma and local motor potentials for movement preparation and execution. *Brain-Computer Interfaces*, 3(2):88–102, 2016.
- [47] Ledyard R Tucker. Some mathematical notes on three-mode factor analysis. *Psychometrika*, 31(3):279–311, 1966.
- [48] Frank Wilcoxon. Individual comparisons by ranking methods. In *Breakthroughs in statistics*, pages 196–202. Springer, 1992.
- [49] Mariana P Branco, Simon H Geukes, Erik J Aarnoutse, Nick F Ramsey, and Mariska J Vansteensel. Nine decades of electrocorticography: A comparison between epidural and subdural recordings. *European Journal of Neuroscience*, 57(8):1260–1288, 2023.
- [50] Soumyadipta Acharya, Matthew S Fifer, Heather L Benz, Nathan E Crone, and Nitish V Thakor. Electrocorticographic amplitude predicts finger positions during slow grasping motions of the hand. *Journal of neural engineering*, 7(4):046002, 2010.
- [51] Chao-Hung Kuo, Guan-Tze Liu, Chi-En Lee, Jing Wu, Kaitlyn Casimo, Kurt E Weaver, Yu-Chun Lo, You-Yin Chen, Wen-Cheng Huang, and Jeffrey G Ojemann. Decoding micro-electrocorticographic signals by using explainable 3d convolutional neural network to predict finger movements. *Journal of Neuroscience Methods*, 411:110251, 2024.
- [52] Tobias Pistohl, Andreas Schulze-Bonhage, Ad Aertsen, Carsten Mehring, and Tonio Ball. Decoding natural grasp types from human ecog. *Neuroimage*, 59(1):248–260, 2012.
- [53] Matthew S Fifer, Guy Hotson, Brock A Wester, David P McMullen, Yujing Wang, Matthew S Johannes, Kapil D Katyal, John B Helder, Matthew P Para, R Jacob Vogelstein, et al. Simultaneous neural control of simple reaching and grasping with the modular prosthetic limb using intracranial eeg. *IEEE transactions on neural systems and rehabilitation engineering*, 22(3):695–705, 2013.
- [54] Mariana P Branco, Simon H Geukes, Erik J Aarnoutse, Mariska J Vansteensel, Zachary V Freudenburg, and Nick F Ramsey. High-frequency band temporal dynamics in response to a grasp force task. *Journal of neural engineering*, 16(5):056009, 2019.
- [55] Tianxiao Jiang, Giuseppe Pellizzetti, Priscilla Asman, Dhiego Bastos, Shreyas Bhavsar, Sudhakar Tummala, Sujit Prabhu, and Nuri F Ince. Power modulations of ecog alpha/beta and gamma bands correlate with time-derivative of force during hand grasp. *Frontiers in neuroscience*, 14:100, 2020.
- [56] Nikhilesh Natraj, Daniel B Silversmith, Edward F Chang, and Karunesh Ganguly. Compartmentalized dynamics within a common multi-area mesoscale manifold represent a repertoire of human hand movements. *Neuron*, 110(1):154–174, 2022.
- [57] Steven M Peterson, Zoe Steine-Hanson, Nathan Davis, Rakesh PN Rao, and Bingni W Brunton. Generalized neural decoders for transfer learning across participants and recording modalities. *Journal of Neural Engineering*, 18(2):026014, 2021.
- [58] Georgios Mentzelopoulos, Evangelos Chatzipantazis, Ashwin G Ramayya, Michelle J Hedlund, Vivek P Buch, Kostas Daniilidis, Konrad P Kording, and Flavia Vitalte. Neural decoding from stereotactic eeg: accounting for electrode variability across subjects. *arXiv preprint arXiv:2411.10458*, 2024.
- [59] Christopher Wang, Vignesh Subramaniam, Adam Uri Yaari, Gabriel Kreiman, Boris Katz, Ignacio Cases, and Andrei Barbu. Brainbert: Self-supervised representation learning for intracranial recordings. *arXiv preprint arXiv:2302.14367*, 2023.
- [60] Tessy M Thomas, Daniel N Candrea, Matthew S Fifer, David P McMullen, William S Anderson, Nitish V Thakor, and Nathan E Crone. Decoding native cortical representations for flexion and extension at upper limb joints using electrocorticography. *IEEE Transactions*

on Neural Systems and Rehabilitation Engineering,
27(2):293–303, 2019.